Cellulose (2024) 31:6815–6826
https://doi.org/10.1007/s10570-024-06034-0

ORIGINAL RESEARCH

One-step electrospinning of cellulose acetate/chitosan/TiO_2 fibrous membranes: efficient humic acid removal by synergistic adsorption and photocatalysis

Yirong Zhang · Yixiang Wang

Received: 11 December 2023 / Accepted: 26 June 2024 / Published online: 29 June 2024

Abstract The removal of contaminants in water purification is limited by the adsorption equilibrium, while the efficiency of photocatalytic oxidation is highly dependent on the adsorption process at the surface of photocatalysts. What would happen if photocatalytic oxidation were combined with biopolymer-based adsorbents? In this work, nano-sized TiO_2 was employed as a model photocatalyst and incorporated in our previously developed highly efficient adsorbents - cellulose acetate (CA)/chitosan (CS) fibrous membranes by one-step electrospinning to continuously and synergistically remove humic acid (HA) from aqueous solutions. The effect of TiO_2 contents on the structure and properties of TiO_2-CA/CS composites was studied by scanning electron microscopy (SEM), Fourier transform infrared spectroscopy (FTIR), and tensile testing, and the adsorption-photocatalysis experiment was carried out as a function of TiO_2 content, pH level, fiber composition, and irradiation time. The results indicated that TiO_2 was uniformly fixed in the electrospun CA/CS fibers. When the content of TiO_2 was 2 wt %, the composite fabric exhibited the highest tensile strength (21.84 ± 0.85 MPa) and could continuously remove HA (87.79% in 3 h without obvious saturation or fiber damage) at a low adsorbent dosage of 0.3 g/L. The HA removal efficiency of the TiO_2-CA/CS fibers under UV irradiation was higher than those of TiO_2-CA and CA/CS fibers, which also indicated a successful synergistic strategy.

Keywords Electrospinning · Adsorption · Photodegradation · Synergistic effect · Humic acid removal

Y. Zhang · Y. Wang (✉)
Department of Food Science and Agricultural Chemistry, McGill University,
Ste Anne de Bellevue, Quebec H9X 3V9, Canada
e-mail: yixiang.wang@mcgill.ca

Introduction

The demand for clean and readily available water is increasing, especially in the face of rapid industrialization and population growth. However, challenges for water supply systems, such as climate change, water scarcity, and urbanization, are still evolving. The World Health Organization (WHO) has emphasized that water reuse is becoming an important strategy to address the water crisis (WHO, 2022). Water purification is an essential step in effectively implementing this measure into practice. Efforts have been made to develop various water treatment processes, including biological treatment, chemical coagulation, precipitation, membrane separation, oxidation, and adsorption (Marinho et al. 2019; Nidheesh and Singh 2017; Roy and Saha 2021; Yadav et al. 2019; Zhang et al. 2008a, 2021b). Among them, adsorption is often considered superior to many other water treatment processes because the design of adsorbents

is facile and it is easy to operate the adsorption equipment (Qiu et al. 2020). Our previous work demonstrated an efficient biodegradable electrospun cellulose acetate (CA)/chitosan (CS) fibrous adsorbent for humic acid (HA) removal. However, it reached the maximum adsorption capacity after 1 h (Zhang et al. 2021a). Replacing or regenerating adsorbents can be a time-consuming and costly process. Numerous other approaches have been proposed to address the accumulation of HA in aqueous environments. These include aluminum salt coagulation of HA (Liu et al. 2009; Sudoh et al. 2015), electrochemical combustion of HA (Liao et al. 2008), ultrafiltration membrane separation (Szymański et al. 2016), and gamma radiation treatment (Sasaki et al. 2018). The treatment processes were often limited in terms of removal efficiency, material and energy consumption, and management of residuals and by-products (Tung et al. 2019).

Heterogeneous photocatalysis employing semiconductor titanium dioxide (TiO_2) exhibited high efficacy for in-suit HA degradation (Birben et al. 2017; Liu et al. 2014; Tung et al. 2019). The remarkable photoactivity, chemical stability, non-toxicity, and abundance of TiO_2 have brought it tremendous attention for environmental remediation (Khorsandi et al. 2015). However, the use of powdery TiO_2 in water treatment can be challenging due to its tendency of agglomeration and subsequent reduced photocatalytic activities (Gebru and Das 2017; Wang et al. 2013). It was also observed that the solution opacity increased at a higher catalyst concentration, leading to a reduction of light penetration (Tung et al. 2019). Additional steps such as coagulation and sedimentation are required for recovery and reuse, which increase the risk of secondary contamination in the water system (Xu et al. 2013). Electrospinning is a facile and versatile technology for generating ultrafine fibrous membranes with large surface-to-volume ratios, which are desirable and reliable substrates for TiO_2 immobilization (Marinho et al. 2021). Enclosing the photocatalysts within such a membrane can overcome the aforementioned limitations and facilitate the reuse of photocatalysts in subsequent cycles. Additionally, the nature of the photocatalytic process is surface-oriented, and the efficiency of photo-oxidation is inseparable from the initial adsorption of the targeted contaminants onto the surface of photocatalysts (Rahman et al. 2021; Rao et al. 2016). Previous studies have primarily focused on either the adsorptive or photocatalytic properties of TiO_2 (Bi et al. 2021; Joung et al. 2006; Liao et al. 2012; Zhang et al. 2008b). It is hypothesized that by incorporating TiO_2 into CA/CS membranes via one-step electrospinning, the CA/CS matrix can provide a large active surface area and high affinity for the adsorption of HA, facilitating subsequent surface-oriented photodegradation of HA, while TiO_2 nanoparticles fixed in the fibers can oxidize the adsorbed HA by creating reactive oxygen species (ROS) to enable the postponed saturation point of the membrane and higher removal capacity. Therefore, this study intends to explore the synergistic effects of adsorption and photooxidation processes facilitated by TiO_2 within the electrospun CA/CS matrix, which have been seldom reported in the context of HA removal and biopolymer-based fibers. The morphological and structural properties of electrospun TiO_2-CA/CS fibers were studied and characterized by scanning electron microscopy (SEM) and Fourier transform infrared (FT-IR) spectroscopy. The impacts of TiO_2 content, pH level, fiber composition, and reaction conditions on the removal of HA were examined, and the synergistic effect of surface adsorption and photocatalytic oxidation was confirmed by comparing the removal efficiencies of TiO_2-CA, TiO_2-CA/CS, and CA/CS fibers. By combining traditional membrane adsorption with nanomaterial catalysis, this work is expected to inspire new ideas for the rational design of efficient adsorbents for water treatment.

Experimental methods

Materials

Cellulose acetate (CA) tow that is used to produce cigarette filters was kindly provided by Celanese Corporation (Irving, US) with a molecular weight of 75–95 kDa, acetyl content of 39.95 wt %, and degree of substitution of ~2.47. Chitosan (CS) synthesized from crab shell with a molecular weight of 190–310 kDa and degree of deacetylation of 75–85%, was provided by Dr. Benjamin Simpson (Department of Food Science and Agricultural Chemistry, McGill University, Quebec, Canada). Acetic acid (CH_3COOH, glacial), humic acid (sodium salt, $C_9H_8Na_2O_4$ 45–70%), titanium dioxide (TiO_2, particle size of ~20 nm),

sodium hydroxide (NaOH, ACS reagent grade), and sulfuric acid (H_2SO_4, ACS reagent grade) were all purchased from Fisher Scientific (Mississauga, ON, Canada) and used as received without further purification. Deionized water was used throughout all experiments.

One-step electrospinning of TiO_2-CA/CS fibrous membranes

Desired amounts of CA and CS were dissolved in 85 wt % acetic acid solution and stirred for 48 h. Different amounts of TiO_2 nanoparticles were also dispersed in 85 wt % acetic acid solution by using Vortex at 3000 rpm, and the suspensions were subsequently sonicated for 90 min and added into the CA/CS solutions, which were placed in the sonication bath for another 90 min. The prepared TiO_2-CA/CS composite solutions were forced through a stainless-steel needle with a diameter of 0.66 mm, and the fibers were collected on a stainless-steel drum rotating at 10 rpm. Electrospinning conditions were optimized in our preliminary experiment to allow the steady generation of fibers. The summary of sample compositions and the optimized electrospinning conditions is listed in Table 1. The electrospun fabrics were vacuum-dried in a desiccator at room temperature overnight to expel possible solvent residues. In order to confirm the synergistic effect of photocatalysis and adsorption, electrospun TiO_2-CA fibrous membranes were prepared by the same method as abovementioned.

Characterization of TiO_2-CA/CS fibrous membranes

Morphological observation of TiO_2-CA/CS fibrous membranes was done using a Hitachi SU-3500 SEM (Hitachi, Tokyo, Japan) operating at 30 kV. All samples were coated with 4 nm of platinum/gold layers using a Leica EM ACE200 coater (Leica, Wetzlar, Germany) prior to the observation. To measure the fiber diameters, SEM images of various samples under a magnification of ×10 k were selected from which four hundred random positions were measured for each sample using the ImageJ image-visualization software (developed by the National Institute of Health) (Wang et al. 2017). The chemical structure of the electrospun fibers was analysed with a Varian Excalibur 3100 FT-IR spectrometer (Varian, Melbourne, Australia) equipped with an attenuated total reflectance accessory (Specac, Orpington, UK). Each FT-IR spectrum was recorded in transmittance mode as the average of 64 scans with a resolution of 4 cm^{-1}. Uniaxial tensile testing of the fibrous membranes was carried out on an ADMET eXpert 7601 testing machine (ADMET, Norwood, MA, USA) at the fixed initial grip-separation distance of 10 mm and crosshead velocity of 1 mm min^{-1}. Five specimens with dimensions of 30 mm × 10 mm (length × width) from each sample were measured according to the ASTM D-638-V standard (Selling et al. 2011). The thickness of each sample was measured from SEM images using the ImageJ image-visualization software. The tensile strength (σ) of the electrospun membranes was determined and calculated from the following equation:

$$\sigma = \frac{F}{A} \tag{1}$$

Synergistic removal of HA

The performance of TiO_2-CA/CS fibrous membranes towards HA removal was investigated by batch experiments. The removal rate of HA was determined as the functions of TiO_2 content, treatment time, and pH level of the solution under the optimized conditions

Table 1 Solution compositions and optimized electrospinning conditions of various fibrous membranes

Samples	CA content (wt %)	CS content (wt %)	TiO_2 content (wt %)	Electrospinning conditions		
				Applied voltage (kV)	Tip-to-collector distance (cm)	Flow rate (mL h^{-1})
1%TiO_2-CA/CS	3	3	1	23.5	11.5	1
2%TiO_2-CA/CS	3	3	2	26	11.5	1.2
3%TiO_2-CA/CS	3	3	3	30	10	1.6
TiO_2-CA	11	0	2	20	12	0.8

as follows: membrane dosage of 0.3 g L^{-1} (approximately 20 mm × 10 mm, length × width), HA solution volume of 20 mL, HA initial concentration of 30 ppm, and stirring speed of 150 rpm (Zhang et al. 2021a). Stock solution with a concentration of 100 ppm HA was prepared and further diluted to obtain HA solutions with lower concentrations. Sulfuric acid and sodium hydroxide were used to adjust the pH levels of HA solutions. Batch experiments were carried out in 25 mL glass vials, and a 20 W UV lamp with a standard wavelength of 365 nm was used as the light source. The distance between the lamp and the water surface was 10 cm. The performance of the TiO_2-CA/CS membranes towards HA removal in dark conditions was also evaluated. To calculate the HA concentration before and after the treatment, a calibration curve was prepared with a series of standard solutions with known HA concentrations. The UV-vis absorbance of the solutions at 271 nm was measured using a Hitachi UV-2000 UV-vis spectrophotometer (Hitachi, Tokyo, Japan). The removal efficiency was calculated as follows:

$$\text{removal efficiency } (\%) = \frac{(C_0 - C_i)}{C_0} \times 100\% \quad (2)$$

where C_0 (mg/L) is the initial HA concentration in the solution and C_i (mg/L) is the equilibrium HA concentration.

The kinetics of photocatalyzed oxidation were studied by applying and modeling the experimental data into the Langmuir-Hinshelwood kinetic model:

$$\mathrm{r} = -\frac{dC}{dt} = \frac{k_r KC}{1 + KC} \quad (3)$$

where r (mg/ (L min)) represents the rate of reaction that changes with time; C (mg/L) is the concentration of HA solution at time t (min); k_r (mg/(L min)) is the rate constant of the reaction; and K (L/mg) is the equilibrium constant for adsorption of the substrate onto the catalyst. Equation (3) can be integrated between the limits: $C = C_0$ at $t = 0$ and $C = C$ at $t = t$, which is expressed as:

$$\ln\left(\frac{C_0}{C}\right) + K(C_0 - C) = k_r K t \quad (4)$$

where C_0 (mg/L) is the initial HA concentration in the solution (Kumar et al. 2008).

Statistical analysis

Statistical interpretations of the results were evaluated by analysis of variance (ANOVA) followed by multiple comparison tests of the means using Duncan's multiple-range test at a 95% confidence level. All statistical analyses were done using SPSS statistical software (version 27, IBM, Armonk, NY, USA) with a $p < 0.05$ considered to be significant. The results were expressed as the mean of at least three replicates ± standard deviation.

Results and discussion

Structure of TiO_2-CA/CS fibrous membranes

FT-IR was employed to understand the component interactions and characteristic chemical information of TiO_2-CA/CS fibrous membranes. As shown in Fig. 1, all the samples had the characteristic peaks of CA at 3500 cm^{-1}, 1750 cm^{-1}, and 1372 cm^{-1} (representing O-H stretching, C=O vibration, and CH_3 groups of the acetyl moiety) (Monisha et al. 2016; Zhang et al. 2021a), and the typical infrared diffraction peaks of CS at 3350 cm^{-1} (-OH and -NH groups) and 1600 cm^{-1}, 1100 cm^{-1}, and 885 cm^{-1} (amine groups) (Sharaf et al. 2021). Compared to the spectrum of TiO_2-CA, all the other samples showed downfield shifts from the peak at 3500 cm^{-1} to the

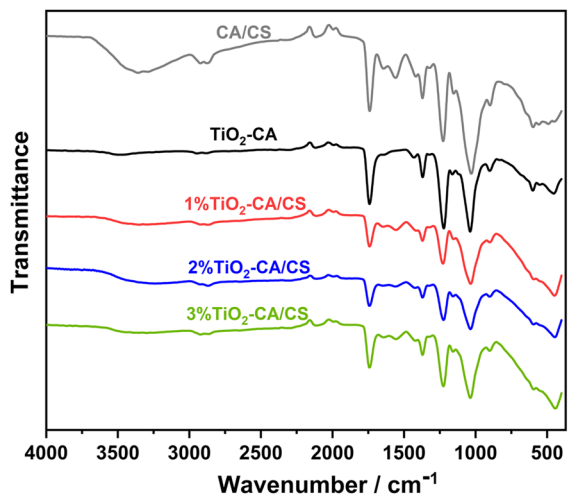

Fig. 1 FTIR spectra of CA/CS, TiO_2-CA, 1%TiO_2-CA/CS, 2%TiO_2-CA/CS, and 3%TiO_2-CA/CS electrospun fibers

broad peak at 3350 cm^{-1}, which revealed the hydrogen bonding interactions between the amine groups of CS and acetyl groups of CA (Gopi et al. 2019). After introducing TiO_2 nanoparticles, TiO_2-CA and TiO_2-CA/CS fibers exhibited new and similar adsorption patterns in the wavenumber range of 350 cm^{-1} to 750 cm^{-1}, which was assigned to the vibration of Ti-O-Ti network and confirmed the successful incorporation of TiO_2 into the CA/CS fibrous matrix (Tsiourvas et al. 2011). However, the change in TiO_2 contents didn't affect the intensities of the characteristic peaks, suggesting that the incorporation of TiO_2 nanoparticles did not significantly impact the structure of CA/CS fibers.

To investigate the effect of TiO_2 on the electrospun fibers, the morphologies of the fabrics with various compositions were observed by SEM and the images are shown in Fig. 2. All the samples exhibited ultrafine and continuous fibrous structures with nano-scaled diameters, which are highly desirable for the adsorption and photocatalysis processes (Erhayem and Sohn 2014; Liu et al. 2014; Lv et al. 2011). The average fiber diameters of 1%TiO_2-CA/CS, 2%TiO_2-CA/CS, and 3%TiO_2-CA/CS were 16.0 ± 7.7, 12.6 ± 4.2, and 15.08 ± 8.2 nm, respectively, and were much smaller than those of TiO_2-CA (149.9 ± 39.2 nm) and the electrospun CA/CS fibers reported in our previous study (Zhang et al. 2021a). It might be due to the higher voltage applied, the shorter tip-to-collector distances, and consequently the enhanced electrical field during electrospinning, resulting in a better stretch of the fibers (He et al. 2015; Kiennork et al. 2015). It was observed that more concave/convex fibers and beads were presented in the 3% TiO_2-CA/CS sample. These were caused by the formation of an unstable Taylor cone in the presence of high TiO_2 loading amounts and the possible agglomeration of the nanoparticles (Gebru and Das 2017; Zhang et al. 2021b).

Mechanical properties of TiO_2-CA/CS fibrous membranes

As shown in Fig. 3, the tensile strength of 1%TiO_2-CA/CS, 2%TiO_2-CA/CS, and 3%TiO_2-CA/CS were 19.02 ± 0.91, 21.84 ± 0.85, and 13.02 ± 1.01, respectively. The addition of TiO_2 nanoparticles to the CA/CS matrix remarkably improved the tensile strength (Zhang et al. 2021a). It could be explained by the transfer and diversion of force from the CA/CS fibers to the nanoparticles, and the stable interface between TiO_2 and the CA/CS matrix (Habiba et al. 2019; Kochkina and Butikova 2019). The significantly higher tensile strength of the 2%TiO_2-CA/CS sample corresponded to its homogeneous fibrous structure and well-dispersed TiO_2 nanoparticles, resulting in better stress distribution and energy absorption (Feng et al. 2019; Zhang et al. 2021a). All the TiO_2-CA/CS membranes demonstrated higher tensile strength than that of the TiO_2-CA sample (2.19 ± 0.17 MPa). It can be attributed to the hydrogen bonding interactions between the amine groups of CS and the acetyl groups of CA that contributed to the retardation of loading stress (Han et al. 2019). However, the introduction of TiO_2 had a negative impact on the strain of the TiO_2-CA/CS membranes. With the increase of the TiO_2 contents from 1 wt % to 3 wt %, the elongation at break of the membranes reduced considerably from 1.61 ± 0.11% to 0.98 ± 0.07%, because the TiO_2 nanoparticles restrained the matrix flexibility and mobility. Similar phenomena were reported in TiO_2-reinforced starch-based nanocomposite films (Oleyaei et al. 2016).

Removal of HA

Effect of pH

The effect of initial solution pH on HA removal using electrospun TiO_2-CA/CS membranes was investigated within a pH range of 4 to 12. Experiments conducted at $pH < 4$ were excluded due to the coagulation and precipitation of HA (Abate and Masini 2003; Brigante et al. 2007; Zhang et al. 2021a). As depicted in Fig. 4, the synergistic removal efficiency of HA using TiO_2-CA/CS was pH-dependent and increased at lower pH values. The p*Ka* values of HA and the primary amine of CS were approximately 4.0 and 6.5, respectively, and the point of zero charge value of TiO_2 falls within a pH range of 6.0 to 7.5 (Laird and Koskinen 2008; Mohammed et al. 2017; Paz 2006). Therefore, at $pH = 4$, electrostatic attraction occurred between the deprotonated carboxylic groups of HA and the positively charged CS and TiO_2 nanoparticles, contributing to the superior removal efficiency towards HA. Meanwhile, the nonpolar methyl groups of CA interacted with the

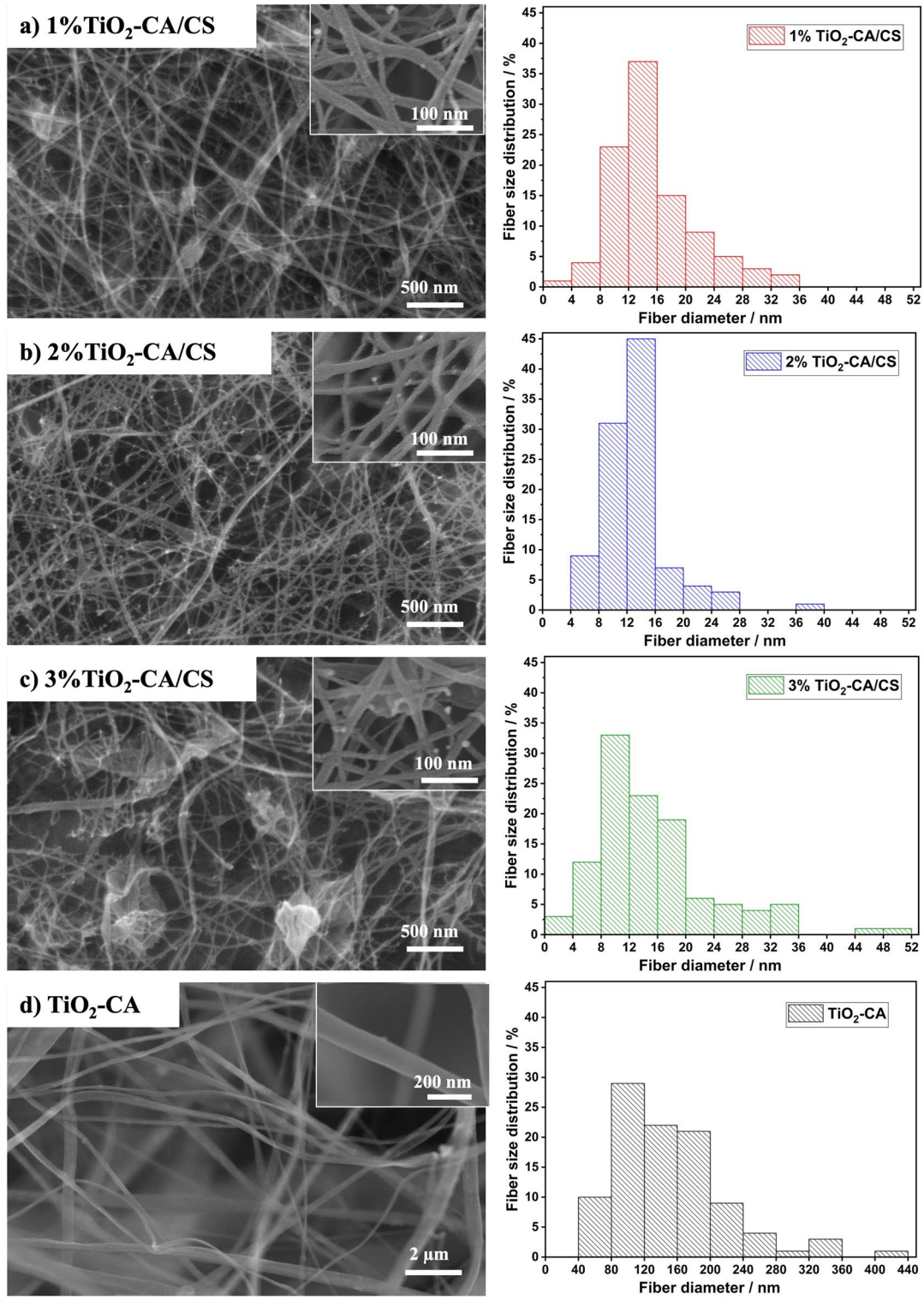

Fig. 2 SEM images and fiber diameter distributions of (**a**) 1%TiO_2-CA/CS, (**b**) 2%TiO_2-CA/CS, (**c**) 3%TiO_2-CA/CS, and (**d**) TiO_2-CA electrospun fibers

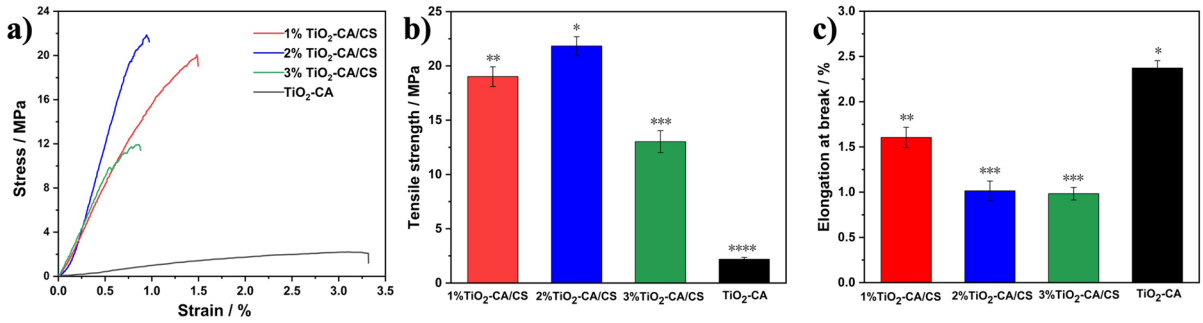

Fig. 3 Mechanical properties of the electrospun fibrous membranes: (**a**) stress-strain curves, (**b**) tensile strength, and (**c**) elongation at break. Different asterisks on the top of each column represent significant differences ($p < 0.05$)

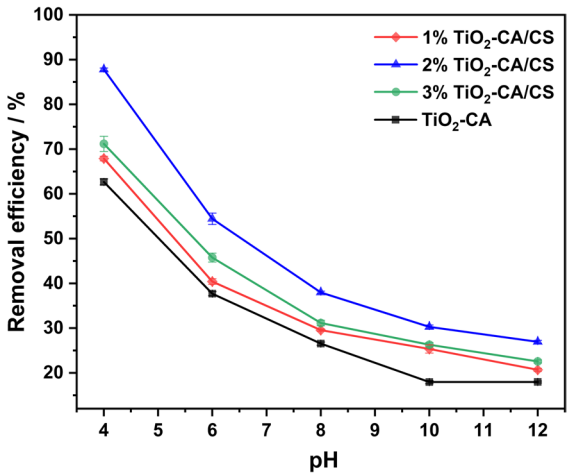

Fig. 4 Effect of pH on the removal of HA using electrospun TiO_2-CA/CS and TiO_2-CA fibrous membranes (dosage: 0.3 g/L; initial concentration of HA solution: 30 ppm; volume: 20 mL; and irradiation time: 180 min)

hydrophobic moieties of HA through hydrophobic interaction, and the positive charges of TiO_2 were favorable for transferring photo-generated electrons to the surface of TiO_2 and discouraging the recombination of photoelectrons and photoholes, leading to the prolonged generation of ROS (Xue et al. 2011). It was worth noting that the 2%TiO_2-CA/CS sample showed the highest removal efficiency towards HA at all pH levels, while the TiO_2-CA fibers were the least efficient. It confirmed that the strong adsorption of HA onto the surface of the electrospun fibers was highly conducive to the photocatalytic process (Krasian et al. 2019).

Effect of irradiation time

The removal efficiencies of various TiO_2-incorporated fibrous composites under UV irradiation or in the dark as a function of treatment time are illustrated in Fig. 5(a). The synergistic effect of adsorption and photocatalysis was evaluated by comparing with the photocatalysis under UV irradiation without the adsorptive sites of CS and the adsorption of TiO_2-CA/CS fibers in dark conditions. All samples exhibited rapid removal of HA within the first 30 min, implying tremendously available adsorptive sites. The adsorption process typically occurs faster than the photocatalytic oxidation (Liu et al. 2014). As the adsorption process continued, the active sites became increasingly occupied, and the removal efficiencies of the samples in the dark reached the equilibrium after approximately 60 min, which was in accordance with our previous report (Zhang et al. 2021a). The TiO_2-CA membrane adsorbed HA through the hydrophobic interaction between HA and CA and surface complexation of TiO_2 and HA (Sun and Lee 2012). However, its removal efficiency in the dark was the lowest because of the absence of CS. It was noteworthy that 1-3% TiO_2-CA/CS fibrous membranes demonstrated continuous removal of HA from the aqueous solution under UV irradiation, and the removal efficiencies were approximately 1.5 times higher than those achieved by adsorption solely within 180 min. Moreover, the removal efficiency of TiO_2-CA with UV irradiation was also lower than those of the 1-3% TiO_2-CA/CS membranes, demonstrating the remarkable synergistic effect of the adsorption process and photocatalytic

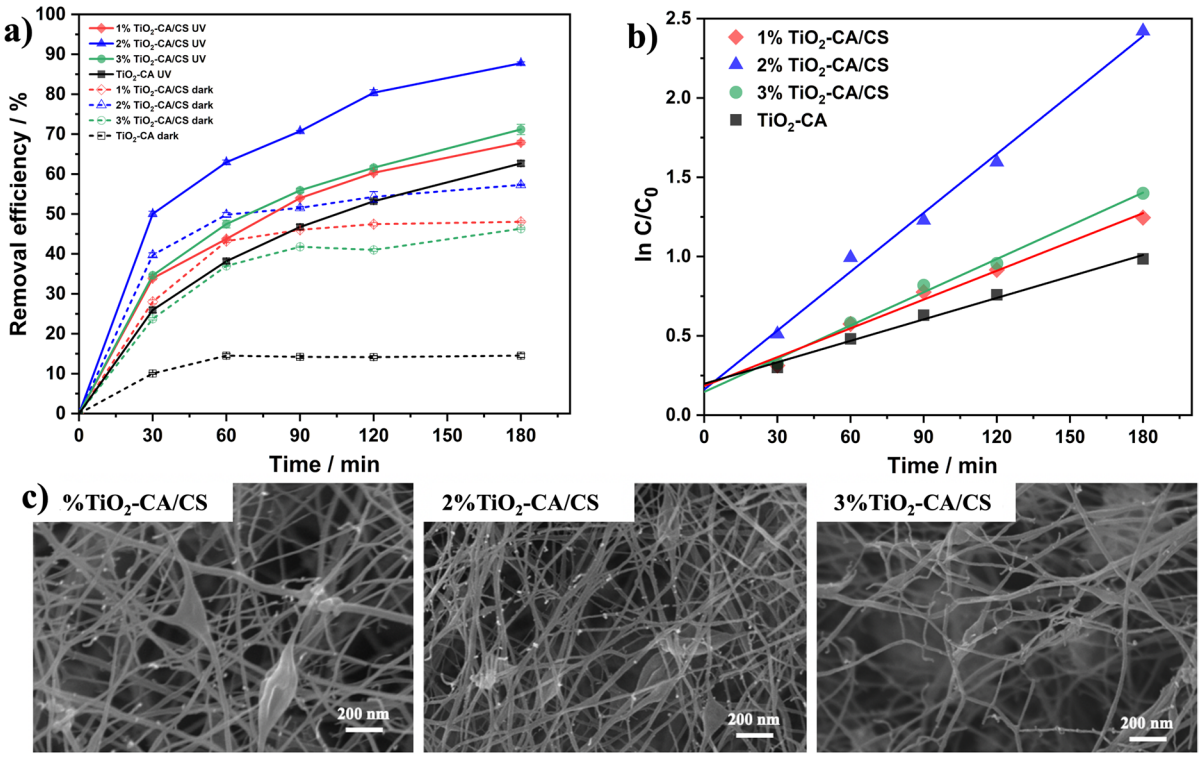

Fig. 5 (**a**) Removal efficiency of TiO_2-incorporated fibers with various compositions under UV irradiation or in dark, (**b**) kinetics of HA removal using TiO_2-incorporated fibers (pH: 4.0; dosage: 0.3 g/L; initial concentration of HA solution: 30 ppm; volume: 20 mL), and (**c**) SEM images of TiO_2-CA/CS fibers after 180 min UV irradiation

activity towards the removal of HA. The 2% TiO_2-CA/CS sample exhibited the highest efficiency due to the uniform fibrous structure, which facilitated the adsorption and degradation of HA. Table 2 summarizes several TiO_2-incorporated photocatalysts for HA removal, and the fibrous TiO_2-CA/CS membranes reported here showed a comparable removal efficiency at a lower dosage of 0.3 g/L.

Kinetics of HA removal

To examine and compare the removal rates of HA using various TiO_2-incorporated fibrous composites, the experimental data were fitted into the Langmuir-Hinshelwood kinetic model, which is the most commonly used kinetic expression of the heterogeneous catalytic processes (Kumar et al. 2008). The kinetics

Table 2 List of previously reported TiO_2 based photocatalysts for HA removal

Photocatalysts	Dosage (g/L)	Removal efficiency (%)	Time (min)	References
Molybdenum-doped TiO_2 nanoparticles	2	83	200	(Abedi et al. 2022)
Reduced graphene oxide- TiO_2 nanocomposites	1.2	88.7	180	(Zhou et al. 2019)
Fe-doped TiO_2 nanoparticles	0.4	74	60	(Kamani et al. 2021)
Fe-doped TiO_2@Fe_3O_4	0.4	100	60	(Moein et al. 2020)
N-doped TiO_2 nanotubes/graphene composite film	1	92.3	120	(Wang et al. 2022)
TiO_2-coated ceramic foam		83	720	(Mori et al. 2013)
This study	0.3	87.7	180	

Table 3 Summary of fitted parameters of HA removal using the Langmuir-Hinshelwood kinetic model

Samples	k_r (mg/ (L min))	R^2
1%TiO_2-CA/CS	0.027	0.975
2%TiO_2-CA/CS	0.051	0.992
3%TiO_2-CA/CS	0.029	0.988
TiO_2-CA	0.021	0.961

and fitted parameters are shown in Fig. 5(b) and listed in Table 3, respectively. The obtained square correlation coefficients (R^2) for all the samples were above 0.96, suggesting that the removal of HA using TiO_2-incorporated fibrous membranes was well fitted by the Langmuir-Hinshelwood kinetic model and relied on the synergistic adsorption upon the fibers and oxidation of HA by TiO_2 in the matrix. The 2%TiO_2-CA/CS sample exhibited a noticeably higher constant rate, whereas TiO_2-CA had the lowest constant rate, which further confirmed the superior removal performance of 2%TiO_2-CA/CS and the success of the synergistic strategy. The morphologies of the fibrous composites after 180 min UV irradiation are shown in Fig. 5(c). It was evident that no significant changes in the structural integrity and fibrous morphologies were observed. It demonstrated the stability of the electrospun CA/CS fibers, and the fibrous structure was important for the continuous removal of contaminants and the recovery of TiO_2 nanoparticles (Li et al. 2022).

Conclusions

The hypothesis has been confirmed that, by one-step electrospinning, the TiO_2-CA/CS fibrous membranes could extend the removal of HA from the aqueous solution via synergistic effects of adsorption and photodegradation. The removal efficiency of HA varied at different pH values, TiO_2 loading amounts, and fiber compositions. Due to the ultrafine fibrous morphology, homogeneity, and uniform distribution of TiO_2 catalysts, the 2%TiO_2-CA/CS fibrous membrane exhibited the highest tensile strength and removal efficiency towards HA. With a low fiber dosage of 0.3 g/L, a removal efficiency of 87.7% was achieved under UV irradiation after 180 min, while the sample in the dark could only remove 54.2% of HA and the adsorption reached the equilibrium after 60 min. Hence, this work presents a promising strategy for the development of high-performance adsorbents for wastewater treatment.

Acknowledgments The authors would like to acknowledge financial support from the Fundings. Y.Z. would like to thank the China Scholarship Council (CSC No. 202107970010) for financial support.

Ethical declarations This work does not contain any studies with human participants or animals performed by the authors.

Author contributions Conceptualization, Y.W. and Y.Z.; experiments, Y.Z.; writing-original draft preparation, Y.Z.; writing-review and editing, Y.W.; supervision, Y.W. All authors have read and agreed to the published version of the manuscript.

Funding This work was supported by the Natural Sciences and Engineering Research Council of Canada (NSERC RGPIN-2019-04498) and the Natural Sciences and Engineering Research Council of Canada Discovery Launch Supplement (NSERC DGECR-2019-00472).

Data availability No datasets were generated or analysed during the current study.

Declarations

Competing interests The authors declare no competing interests.

References

Abate G, Masini JC (2003) Influence of pH and ionic strength on removal processes of a sedimentary humic acid in a suspension of vermiculite. Colloids Surf a: Physicochem Eng Asp 226:25–34. https://doi.org/10.1016/S0927-7757(03)00418-7

Abedi K, Shahmoradi B, Wantala K, Suwannaruang T, Amini N, Maleki A, Lee SM, Shivaraju HP (2022) Immobilized Mo:TiO_2 nanoparticles for humic acid removal in an aqueous medium using solar spectrum. J Mater Sci: Mater Electron 33:16777–16788. https://doi.org/10.1007/s10854-022-08542-w

Bi L, Chen Z, Li L, Kang J, Zhao S, Wang B, Yan P, Li Y, Zhang X, Shen J (2021) Selective adsorption and enhanced photodegradation of diclofenac in water by molecularly imprinted TiO_2. J Hazard Mater 407:124759. https://doi.org/10.1016/j.jhazmat.2020.124759

Birben NC, Uyguner-Demirel CS, Kavurmaci SS, Gürkan YY, Turkten N, Cinar Z, Bekbolet M (2017) Application of Fe-doped TiO_2 specimens for the solar photocatalytic degradation of humic acid. Catal Today 281:78–84. https://doi.org/10.1016/j.cattod.2016.06.020

Brigante M, Zanini G, Avena M (2007) On the dissolution kinetics of humic acid particles: effects of pH, temperature and Ca^{2+} concentration. Colloids Surf a: Physicochem Eng Asp 294:64–70. https://doi.org/10.1016/j.colsurfa.2006.07.045

Erhayem M, Sohn M (2014) Stability studies for titanium dioxide nanoparticles upon adsorption of Suwannee River humic and fulvic acids and natural organic matter. Sci Total Environ 468–469:249–257. https://doi.org/10.1016/j.scitotenv.2013.08.038

Feng S, Zhang F, Ahmed S, Liu Y (2019) Physico-Mechanical and Antibacterial properties of PLA/TiO_2 Composite materials synthesized via Electrospinning and Solution casting processes. Coatings 9:525. https://doi.org/10.3390/coatings9080525

Gebru KA, Das C (2017) Removal of pb (II) and Cu (II) ions from wastewater using composite electrospun cellulose acetate/titanium oxide (TiO_2) adsorbent. J Water Process Eng 16:1–13. https://doi.org/10.1016/j.jwpe.2016.11.008

Gopi S, Pius A, Kargl R, Kleinschek KS, Thomas S (2019) Fabrication of cellulose acetate/chitosan blend films as efficient adsorbent for anionic water pollutants. Polym Bull 76:1557–1571. https://doi.org/10.1007/s00289-018-2467-y

Habiba U, Lee JJL, Joo TC, Ang BC, Afifi AM (2019) Degradation of methyl orange and Congo red by using chitosan/polyvinyl alcohol/TiO_2 electrospun nanofibrous membrane. Int J Biol Macromol 131:821–827. https://doi.org/10.1016/j.ijbiomac.2019.03.132

Han X, Ye Y, Lam F, Pu J, Jiang F (2019) Hydrogen-bonding-induced assembly of aligned cellulose nanofibers into ultrastrong and tough bulk materials. J Mater Chem 7:27023–27031. https://doi.org/10.1039/C9TA11118B

He X, Cheng L, Zhang X, Xiao Q, Zhang W, Lu C (2015) Tissue engineering scaffolds electrospun from cotton cellulose. Carbohydr Polym 115:485–493. https://doi.org/10.1016/j.carbpol.2014.08.114

Joung S, Amemiya K, Murabayashi M, Itoh K (2006) Adsorbed species on TiO2 associated with the photocatalytic oxidation of trichloroethylene under UV. J Photochem Photobiol A: Chem 184:273–281. https://doi.org/10.1016/j.jphotochem.2006.04.040

Kamani H, Ashrafi SD, Jahantiq A, Norabadi E, Dashti Zadeh M (2021) Catalytic degradation of humic acid using Fe–doped TiO_2 - ultrasound hybrid system from aqueous solution. Int J Environ Anal Chem 103:8017–8031. https://doi.org/10.1080/03067319.2021.1979535

Khorsandi H, Bina B, Khorsandi J (2015) Evaluation of UV/TiO_2 photo-catalytic process for removing Humic compounds from Water. Pol J Environ Stud 24:1063–1068

Kiennork S, Nakhowong R, Chueachot R, Tipparach U (2015) Preparation and characterization of Electrospun TiO_2 nanofibers via Electrospinning. Integr Ferroelectr 165:131–137. https://doi.org/10.1080/10584587.2015.1063915

Kochkina NE, Butikova OA (2019) Effect of fibrous TiO_2 filler on the structural, mechanical, barrier and optical characteristics of biodegradable maize starch/PVA composite films. Int J Biol Macromol 139:431–439. https://doi.org/10.1016/j.ijbiomac.2019.07.213

Krasian T, Punyodom W, Worajittiphon P (2019) A hybrid of 2D materials (MoS_2 and WS_2) as an effective performance enhancer for poly(lactic acid) fibrous mats in oil adsorption and oil/water separation. Chem Eng J 369:563–575. https://doi.org/10.1016/j.cej.2019.03.092

Kumar KV, Porkodi K, Rocha F (2008) Langmuir–Hinshelwood kinetics – a theoretical study. Catal Commun 9:82–84. https://doi.org/10.1016/j.catcom.2007.05.019

Laird DA, Koskinen WC (2008) Chap. 21 - triazine soil interactions. In: LeBaron HM, McFarland JE, Burnside OC (eds) The Triazine Herbicides, 1st edn. Elsevier, Amsterdem, pp 275–299. https://doi.org/10.1016/B978-0444511167-6.50024-6

Li W, Zhang H, Chen W, Yang L, Wu H, Mao N (2022) The effects of cotton cellulose on both energy band gap of g-C_3N_4–TiO_2 nanoparticles and enhanced photocatalytic properties of cotton-g-C_3N_4–TiO_2 composites. Cellulose 29:193–212. https://doi.org/10.1007/s10570-021-04318-3

Liao AA, Spitzer M, Motheo AJ, Bertazzoli R (2008) Electrocombustion of humic acid and removal of algae from aqueous solutions. J Appl Electrochem 38:721–727. https://doi.org/10.1007/s10800-008-9502-x

Liao J, Lin S, Pan N, Li D, Li S, Li J (2012) Free-standing open-ended TiO2 nanotube membranes and their promising through-hole applications. Chem Eng J 211–212:343–352. https://doi.org/10.1016/j.cej.2012.09.070

Liu H, Hu C, Zhao H, Qu J (2009) Coagulation of humic acid by PACl with high content of Al13: the role of aluminum speciation. Sep Purif Tech 70:225–230. https://doi.org/10.1016/j.seppur.2009.09.020

Liu S, Lim M, Amal R (2014) TiO_2-coated natural zeolite: Rapid humic acid adsorption and effective photocatalytic regeneration. Chem Eng Sci 105:46–52. https://doi.org/10.1016/j.ces.2013.10.041

Lv T, Pan L, Liu X, Lu T, Zhu G, Sun Z (2011) Enhanced photocatalytic degradation of methylene blue by ZnO-reduced graphene oxide composite synthesized via microwave-assisted reaction. J Alloys Compd 509:10086–10091. https://doi.org/10.1016/j.jallcom.2011.08.045

Marinho BA, Cristóvão RO, Boaventura RAR, Vilar VJP (2019) As(III) and cr(VI) oxyanion removal from water by advanced oxidation/reduction processes—a review. Environ Sci Pollut Res 26:2203–2227. https://doi.org/10.1007/s11356-018-3595-5

Marinho BA, de Souza SMAGU, de Souza AAU, Hotza D (2021) Electrospun TiO_2 nanofibers for water and wastewater treatment: a review. J Mater Sci 56:5428–5448. https://doi.org/10.1007/s10853-020-05610-6

Moein H, Nabi Bidhendi G, Mehrdadi N, Kamani H (2020) Efficiency of Photocatalytic Degradation of Humic Acid using magnetic nanoparticles (Fe-doped TiO_2@Fe_3O_4) in Aqueous solutions. Health Scope 9:e102577. https://doi.org/10.5812/jhealthscope.102577

Mohammed MA, Syeda JTM, Wasan KM, Wasan EK (2017) An overview of Chitosan Nanoparticles and its application in Non-parenteral Drug Delivery. Pharmaceutics 9:53. https://doi.org/10.3390/pharmaceutics9040053

Monisha S, Selvasekarapandian S, Mathavan T, Milton Franklin Benial A, Manoharan S, Karthikeyan S (2016) Preparation and characterization of biopolymer electrolyte based on cellulose acetate for potential applications in energy

storage devices. J Mater Sci: Mater Electron 27:9314–9324. https://doi.org/10.1007/s10854-016-4971-x

Mori M, Sugita T, Mase A, Funatogawa T, Kikuchi M, Aizawa K, Kato S, Saito Y, Ito T, Itabashi H (2013) Photodecomposition of humic acid and natural organic matter in swamp water using a TiO_2-coated ceramic foam filter: potential for the formation of disinfection byproducts. Chemosphere 90:1359–1365. https://doi.org/10.1016/j.chemosphere.2012.07.056

Nidheesh PV, Singh TSA (2017) Arsenic removal by electrocoagulation process: recent trends and removal mechanism. Chemosphere 181:418–432. https://doi.org/10.1016/j.chemosphere.2017.04.082

Oleyaei SA, Almasi H, Ghanbarzadeh B, Moayedi AA (2016) Synergistic reinforcing effect of TiO_2 and montmorillonite on potato starch nanocomposite films: Thermal, mechanical and barrier properties. Carbohydr Polym 152:253–262. https://doi.org/10.1016/j.carbpol.2016.07.040

Paz Y (2006) Preferential photodegradation – why and how? C R Chim 9:774–787. https://doi.org/10.1016/j.crci.2005.03.032

Qiu Z, Wang M, Zhang T, Yang D, Qiu F (2020) In-situ fabrication of dynamic and recyclable TiO2 coated bacterial cellulose membranes as an efficient hybrid absorbent for tellurium extraction. Cellulose 27:4591–4608. https://doi.org/10.1007/s10570-020-03096-8

Rahman MM, Huang D, Ewulonu CM, Wang C, Kuga S, Wu M, Huang Y (2021) Preparation of multifunctional cellulosic fabric based on graphene/TiO_2 nanocoating. Cellulose 28:1153–1165. https://doi.org/10.1007/s10570-020-03558-z

Rao G, Zhang Q, Zhao H, Chen J, Li Y (2016) Novel titanium dioxide/iron (III) oxide/graphene oxide photocatalytic membrane for enhanced humic acid removal from water. Chem Eng J 302:633–640. https://doi.org/10.1016/j.cej.2016.05.095

Roy M, Saha R (2021) 6 - Dyes and their removal technologies from wastewater: A critical review. In Bhattacharyya S, Mondal NK, Platos J, Snášel V, Krömer P (Eds), Intelligent Environmental Data Monitoring for Pollution Management, Academic Press, pp. 127–160. https://doi.org/10.1016/B978-0-12-819671-7.00006-3

Sasaki T, Goto R, Saito T, Kobayashi T, Ikuji T, Sugiyama Y (2018) Gamma-ray irradiation impact of humic substances on apparent formation constants with Cu(II). J Nucl Sci Technol 55:1299–1308. https://doi.org/10.1080/00223131.2018.1503573

Selling GW, Woods KK, Biswas A (2011) Electrospinning formaldehyde-crosslinked zein solutions. Polym Int 60(4):537–542. https://doi.org/10.1002/pi.3009

Sharaf SM, Al-Mofty SED, El-Sayed ESM, Omar A, Abo Dena AS, El-Sherbiny IM (2021) Deacetylated cellulose acetate nanofibrous dressing loaded with chitosan/propolis nanoparticles for the effective treatment of burn wounds. Int J Biol Macromol 193:2029–2037. https://doi.org/10.1016/j.ijbiomac.2021.11.034

Sudoh R, Islam MDS, Sazawa K, Okazaki T, Hata N, Taguchi S, Kuramitz H (2015) Removal of dissolved humic acid from water by coagulation method using polyaluminum chloride (PAC) with calcium carbonate as neutralizer and coagulant aid. J Environ Chem Eng 3:770–774. https://doi.org/10.1016/j.jece.2015.04.007

Sun DD, Lee PF (2012) TiO_2 microsphere for the removal of humic acid from water: complex surface adsorption mechanisms. Sep Purif Techol 91:30–37. https://doi.org/10.1016/j.seppur.2011.08.035

Szymański K, Morawski AW, Mozia S (2016) Humic acids removal in a photocatalytic membrane reactor with a ceramic UF membrane. Chem Eng J 305:19–27. https://doi.org/10.1016/j.cej.2015.10.024

Tsiourvas D, Tsetsekou A, Arkas M, Diplas S, Mastrogianni E (2011) Covalent attachment of a bioactive hyperbranched polymeric layer to titanium surface for the biomimetic growth of calcium phosphates. J Mater Sci: Mater Med 22:85–96. https://doi.org/10.1007/s10856-010-4181-7

Tung TX, Xu D, Zhang Y, Zhou Q, Wu Z (2019) Removing Humic Acid from Aqueous Solution using Titanium Dioxide: a review. Pol J Environ 28:529–542. https://doi.org/10.15244/pjoes/85196

Wang X, Wu Z, Wang Y, Wang W, Wang X, Bu Y, Zhao J (2013) Adsorption–photodegradation of humic acid in water by using ZnO coupled TiO_2/bamboo charcoal under visible light irradiation. J Hazard Mater 262:16–24. https://doi.org/10.1016/j.jhazmat.2013.08.037

Wang Y, Yang J, Du R, Chen L (2017) Transition metal ions enable the transition from Electrospun Prolamin Protein Fibers to Nitrogen-Doped Freestanding Carbon films for Flexible Supercapacitors. ACS Appl Mater Interfaces 9:23731–23740. https://doi.org/10.1021/acsami.7b05159

Wang A, Chen W, Geng N, Lan X, Liu M, Wu X (2022) Novel Electrochemical Preparation of N-Doped TiO_2/Graphene for enhanced Stability and Photocatalysis Degradation of Humic Acid. Sustainability 14:10614. https://doi.org/10.3390/su141710614

World Health Organization (WHO) Drinking water challenges. https://www.who.int/news-room/fact-sheets/detail/drinking-water. Accessed 21 May 2022

Xu C, Cui A, Xu Y, Fu X (2013) Graphene oxide–TiO_2 composite filtration membranes and their potential application for water purification. Carbon 62:465–471. https://doi.org/10.1016/j.carbon.2013.06.035

Xue G, Liu H, Chen Q, Hills C, Tyrer M, Innocent F (2011) Synergy between surface adsorption and photocatalysis during degradation of humic acid on TiO_2/activated carbon composites. J Hazard Mater 186:765–772. https://doi.org/10.1016/j.jhazmat.2010.11.063

Yadav M, Gupta R, Sharma RK (2019) Chap. 14 - green and sustainable pathways for Wastewater Purification. In: Ahuja S (ed) Advances in Water purification techniques. Elsevier, pp 355–383. https://doi.org/10.1016/B978-0-12-814790-0.00014-4

Zhang X, Du AJ, Lee P, Sun DD, Leckie JO (2008a) Grafted multifunctional titanium dioxide nanotube membrane: separation and photodegradation of aquatic pollutant. Appl Catal B: Environ 84:262–267. https://doi.org/10.1016/j.apcatb.2008.04.009

Zhang X, Du AJ, Lee P, Sun DD, Leckie JO (2008b) TiO_2 nanowire membrane for concurrent filtration and photocatalytic oxidation of humic acid in water. J Memb Sci 313:44–51. https://doi.org/10.1016/j.memsci.2007.12.045

Zhang Y, Wang F, Wang Y (2021a) Electrospun Cellulose Acetate/Chitosan Fibers for humic acid removal: construction guided by Intermolecular Interaction Study. ACS Appl Polym Mater 3:5022–5029. https://doi.org/10.1021/acsapm.1c00778

Zhang Y, Wang F, Wang Y (2021b) Recent developments of electrospun nanofibrous materials as novel adsorbents for water treatment. Mater Today Commun 27:102272. https://doi.org/10.1016/j.mtcomm.2021.102272

Zhou X, Zhou S, Ma F, Xu Y (2019) Synergistic effects and kinetics of rGO-modified TiO_2 nanocomposite on adsorption and photocatalytic degradation of humic acid. J Environ Manag 235:293–302. https://doi.org/10.1016/j.jenvman.2019.01.026